Energy & Buildings 183 (2019) 749–760

Contents lists available at ScienceDirect

Energy & Buildings

journal homepage: www.elsevier.com/locate/enbuild

Integrating climate change into meteorological weather data for building energy simulation

Sleiman Farah[a,*], David Whaley[a], Wasim Saman[a], John Boland[b]

[a] University of South Australia, School of Engineering, Barbara Hardy Institute, Adelaide, Australia
[b] University of South Australia, Centre for Industrial and Applied Mathematics, School of Information Technology & Mathematical Sciences, Barbara Hardy Institute, Adelaide, Australia

ARTICLE INFO

Article history:
Received 28 August 2018
Revised 6 November 2018
Accepted 24 November 2018
Available online 1 December 2018

Keywords:
Climate change
Meteorological weather data
Heatwaves
Extreme weather
Building energy simulation
Space heating and cooling

ABSTRACT

Current and newly built buildings will inevitably experience the effects of climate change, therefore, the design and performance of these buildings should consider weather data that includes some of the effects of climate change, instead of only using historical weather data. However, climate change weather data suitable for buildings performance simulation are typically unavailable. This research presents a method to integrate climate change features into historical weather data to make suitable climate change weather data available for buildings performance simulation. The method separates hourly dry bulb temperature into three time series components to simplify the integration of three climate change features. The method adjusts the maximum and minimum monthly averages, the number of days with maximum temperature above a specified threshold, and the number of consecutive occurrences of days with maximum temperature above a specified threshold (heatwave). The research also presents the adjustment of monthly averages of global solar irradiation. Under the climate–changed weather conditions, the annual heating thermal energy decreases by 21%–22%, the annual cooling thermal energy increases by 29%–31%, and the combined heating and cooling thermal energy decreases by 4%–5% compared to the heating and cooling thermal energy under the current weather conditions. The results indicate that climate–changed weather data is necessary as historical weather data is insufficient for accurately assessing the energy performance of a building.

© 2018 Elsevier B.V. All rights reserved.

1. Introduction

As global temperature continues to rise, the impact of climate change on living species and ecosystems cannot be overstated. Some of the devastating effects of climate change are happening already [1], creating a challenge in combating climate change for current and future generations. Most nations have agreed to reduce greenhouse gas emissions to mitigate the effects of climate change and maintain a relatively low global temperature [2]. However, the global temperature is likely to continue to increase for many decades [3], which means that despite the current efforts to combat climate change, humans will have to find means to adapt to the changing climate.

For the built environment, as existing and newly built buildings are expected to perform over their lifetime which extends for several decades, the buildings design and performance assessment should not be based on current methods that use historical data, but rather should use the predicted future climate. Therefore, developing Typical Meteorological Year (TMY) weather data that includes the effects of climate change is necessary to facilitate proper design and energy performance assessment of buildings.

Several approaches were investigated for integrating climate change into meteorological weather data to simulate buildings energy performance. The approaches can be grouped into extrapolating statistical approach [4], imposed offset approach [5], stochastic weather models [6] and global climate models [7]. Of these groups, the imposed offset approach is the simplest approach that can produce reliable results [8]. The imposed offset approach integrates predicted future climate variation data obtained from global climate models into the meteorological weather data [9,10]. The global climate models use fundamental principles of physics to model the interaction between the atmosphere and the surface of the earth in order to predict the future climate [11]. A comprehensive summary of these approaches can be found in [8].

The most common method that uses the imposed offset approach is the morphing method, which has been used in several studies to include climate change into meteorological weather

* Corresponding author.
E-mail address: sleiman.farah@mymail.unisa.edu.au (S. Farah).

https://doi.org/10.1016/j.enbuild.2018.11.045
0378-7788/© 2018 Elsevier B.V. All rights reserved.

data [12–15]. This method consists of adjusting the time series of weather variables by shifting and stretching [5]. Depending on the desired effect, these adjustments could be applied either separately or combined. For instance, both shifting and stretching are applied to adjust the dry bulb temperature (DBT). The mean DBT is adjusted by shifting, and the diurnal difference between the maximum and minimum DBT is adjusted by stretching [5,13]. The morphing method is relatively easy to implement; however, this method is unable to adjust the maximum and minimum DBT independently, which prohibits the maximum and minimum DBT from being adjusted by different amounts. The morphing method also has a limited number of parameters, which prohibits integrating some climate change features such as extreme temperatures and heatwaves. Currently, extreme temperatures and heatwaves are considered as extreme weather events, therefore, they are not integrated into typical meteorological weather data. However, the effects of climate change will make these events become a more prevalent feature of the future weather [16,17].

This review reveals that the morphing method is limited and unable to integrate important climate change features into meteorological weather data. This paper resolves the aforementioned limitations by presenting a method based on time series analysis to integrate three climate change features of DBT that cannot be integrated by the morphing method:

- Feature One — Increase of average maximum and minimum DBT by different amounts,
- Feature Two — Adjustment of the number of extreme days,
- Feature Three — Integration of heatwave characteristics.

The method presented separates the DBT into three components: a Fourier Series (FS), an autoregressive (AR)–moving average (MA) model, and residuals. The FS model of the DBT is extracted from the original DBT data, and the residuals of the FS are separated into an ARMA model and further residuals. For the development of climate change weather data, the three components are added after applying necessary modifications to the FS model and randomly sampling the residuals. The details of this method are presented in Section 2. For completeness, Section 2 also includes the integration of projected solar irradiation due to climate change and the calculation of diffuse and direct normal irradiation. Using the original and climate–changed weather data, the paper presents an energy simulation of a house to analyse the effect of climate change on space heating and cooling.

2. Methodology

The weather data used in this research to demonstrate the integration of climate change features is the Reference Meteorological Year Climate File 2016 for the City of Adelaide, Commonwealth of Australia (personal communication, August 24, 2017). This weather data is developed by the nationwide house energy rating scheme (NatHERS) that is used to evaluate the thermal performance and star rating of new residential buildings in Australia [18]. The weather data is developed from 26 years of historical weather data (1990–2015) using Finkelstein–Schafer statistics for historical data selection, similar to the development of the commonly known TMY weather data [19].

2.1. Dry bulb temperature

2.1.1. Fourier series model

The development of the FS model is based on the analysis of the power spectrum shown in Fig. 1. The power spectrum shows significant power corresponding to the cycles (N) 1 and 365. These cycles are included in the FS model as the fundamental cycle, N = 1, represents the seasonal DBT variation, and the second cycle, N = 365, represents the daily DBT variation. The power spectrum also shows less significant power for several N values close to the fundamental cycle. These cycles are excluded from the FS as they do not have a reasonable physical interpretation. Nevertheless, the power spectrum also shows a relatively small power corresponding to N = 730. Unlike the other less significant cycles, this cycle is distant from other significant cycles and captures DBT half–daily variation, which could be correlated with the half–daily atmospheric pressure cycle [20].

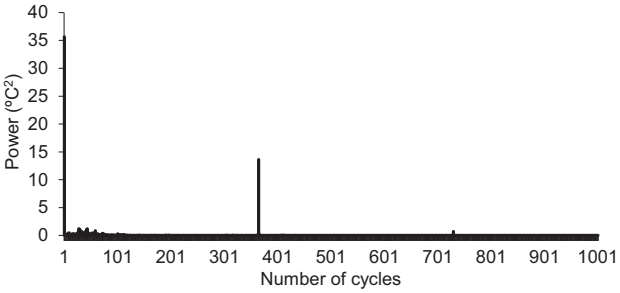

Fig. 1. Dry bulb temperature power spectrum.

Table 1
Fourier series parameters.

i	a_i (°C)	b_i (°C)	ω_i (h^{-1})
1	5.52	2.29	$2\pi/8760$
2	−1.84	−3.20	$365 \times 2\pi/8760$
3	0.18	0.83	$730 \times 2\pi/8760$

Therefore, a three–frequency FS model is fitted to the DBT data as shown in Eq. (1)

$$FS_{DBT} = \overline{DBT} + \sum_{i=1}^{3} (a_i \cos(\omega_i t) + b_i \sin(\omega_i t)) \quad (1)$$

where the mean DBT, $\overline{DBT}$, is equal to 17.0 °C, the FS parameters a_i, b_i, and w_i are summarised in Table 1, and time variable t varies from 1–8760 h. The values a_i and b_i are calculated by minimising the sum of the squared differences between the original DBT data and the FS model.

The daily average DBT of the FS is able to capture the seasonal temperature variation of the original DBT as shown in Fig. 2. The temperature decreases slowly as the season changes from summer (Dec–Feb) to winter (Jun–Aug), and then increases steadily as the season changes from winter to summer. The original DBT fluctuates around the FS while following a trend similar to that of the FS as the season changes.

Similarly, the hourly DBT of the FS captures the daily temperature variation of the original DBT as shown in Fig. 3. The FS shows a consistent daily cycle that matches the daily cycles of the original DBT. Nevertheless, the daily cycles of the original DBT occur either above or below the FS cycles. This pattern is consistent with the daily average DBT where the original DBT fluctuates around the FS as previously shown in Fig. 2. These results demonstrate that the average trend of the original DBT is properly represented by the developed FS model. The differences between the original DBT and the FS model are the residuals of the FS model which are used to build the ARMA model.

2.1.2. Autoregressive–moving average model

The residuals of the FS (FSR), shown in Fig. 4, contain stochastic components which can be identified by analysing both the autocorrelation function (ACF) and the partial autocorrelation function (PACF), shown in Figs. 5 and 6 respectively. The ACF shows relatively slow autocorrelation decay, and the PACF shows a small cy-

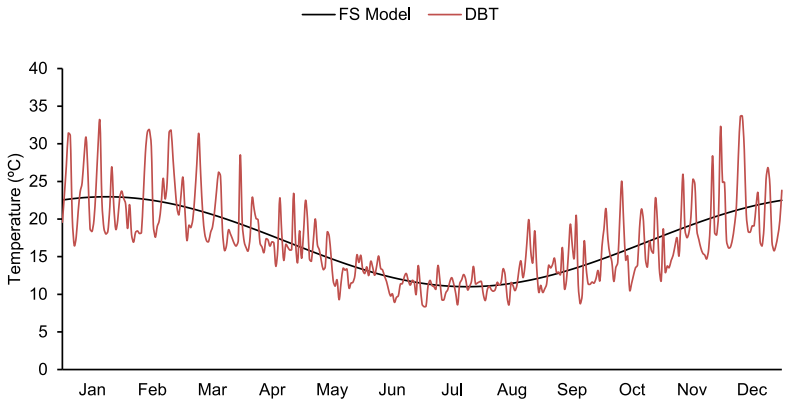

Fig. 2. Comparison between Fourier Series model and original dry bulb temperature (daily average profile).

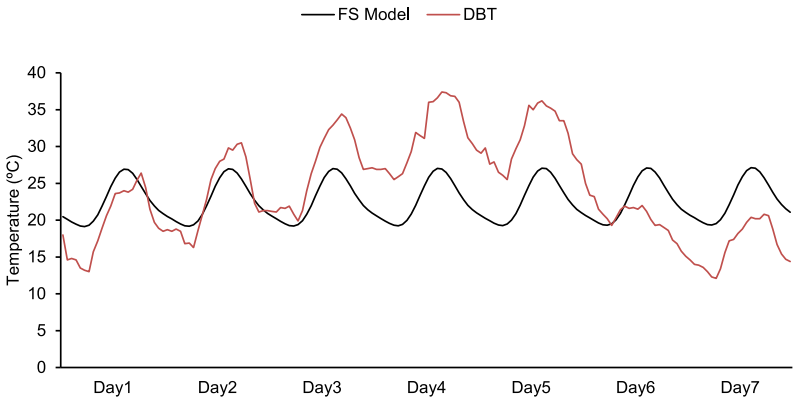

Fig. 3. Comparison between Fourier Series model and original dry bulb temperature (hourly profile for one week).

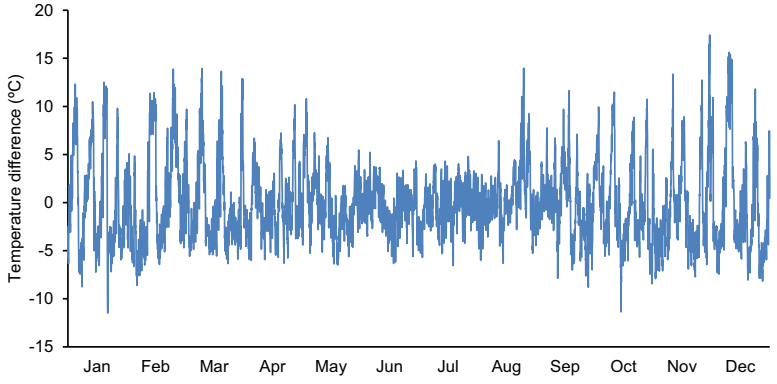

Fig. 4. Dry bulb temperature residuals of the Fourier Series.

cling pattern. These ACF and PACF do not clearly indicate whether an ARMA or an AR model is the most suitable to fit the FSR. Therefore, ARMA and AR models are fitted separately to the FSR using the statistical software Minitab. The aim from fitting these models to the FSR is to identify the most suitable model, i.e. one that has the lowest sum of the squared residuals. The sum of the squared residuals of the best ARMA model, ARMA(1,2), that fits the FS residuals is 712477 $°C^2$, while the sum of the square residuals of the best AR model, AR(4), is 712382 $°C^2$.

This result indicates that the fourth degree AR model, shown in Eq. (2), fits the FSR slightly better than the ARMA(2,1) model. The coefficients of the AR model and their corresponding p–values are shown in Table 2, where all the p–values are significantly lower than 0.05. The *p*–values indicate that the null hypothesis, coefficients equal to zero, is rejected. A one–week sample shows that the AR fits follow the variations of the FS residuals as shown in Fig. 7. This result reveals that the adopted AR model is suitable to represent the variations of the FS residuals.

Table 2
Autoregressive model parameters.

i	α_i	p–value
1	1.2207	< 0.001
2	−0.2142	< 0.001
3	−0.0746	< 0.001
4	0.0360	0.001

$$DBT^t_{FSR} = \sum_{i=1}^{4} \alpha_i DBT^{t-i}_{FSR} + DBT^t_{ARR} \quad (2)$$

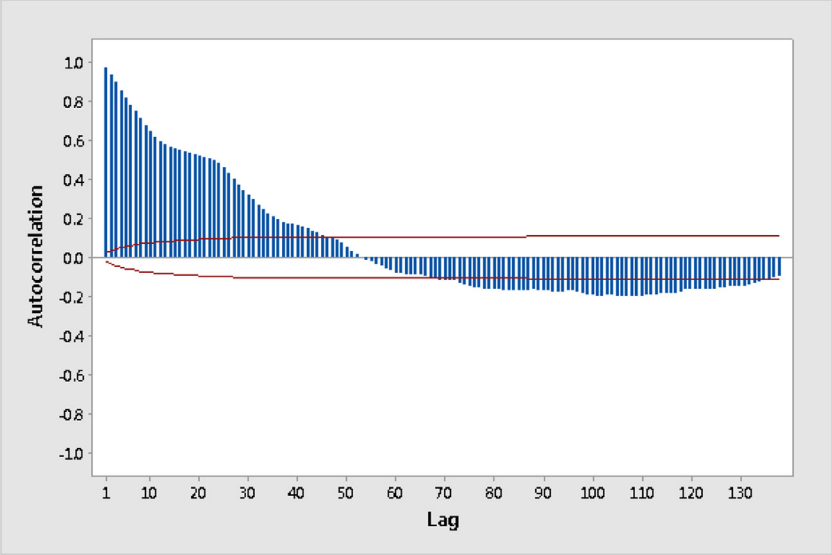

Fig. 5. Autocorrelation function of dry bulb temperature Fourier series residuals.

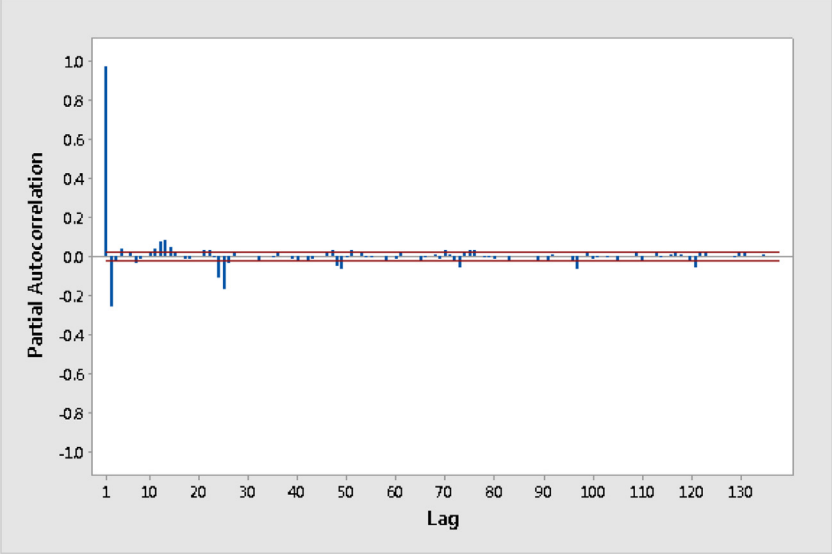

Fig. 6. Partial autocorrelation function of dry bulb temperature Fourier series residuals.

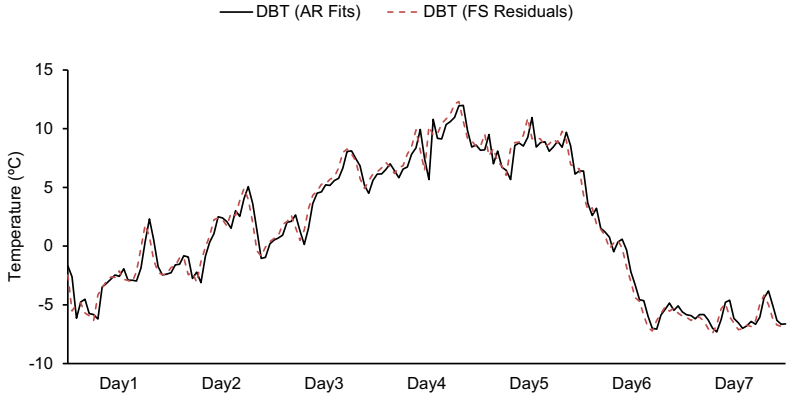

Fig. 7. Comparison between autoregressive fits and Fourier series residuals of dry bulb temperature (hourly profile for a randomly selected week).

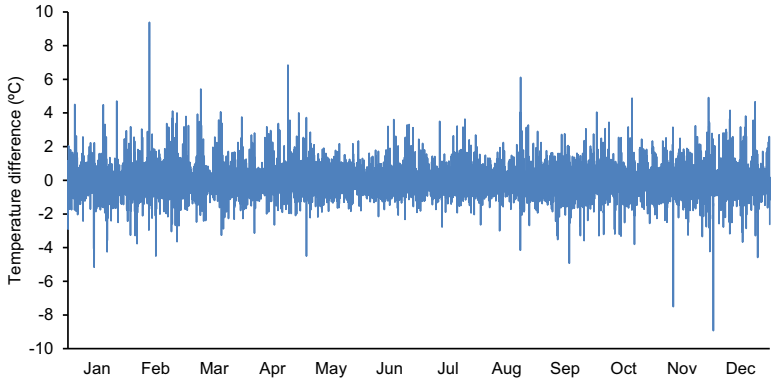

Fig. 8. Dry bulb temperature residuals of the autoregressive model.

Table 3
Predicted increase of monthly average of maximum and minimum dry bulb temperatures [21].

	Increase of maximum temperature (°C)	Increase of minimum temperature (°C)
January	1.3	1.2
February	1.3	1.2
March	1.1	1.2
April	1.2	1.1
May	1.2	1.0
June	1.2	0.9
July	1.2	0.9
August	1.2	0.9
September	1.4	1.0
October	1.5	1.1
November	1.5	1.2
December	1.5	1.3

Table 4
Optimised mean dry bulb temperature and Fourier series daily cycle coefficients.

Month	Mean DBT (°C)	a_i (°C)	b_i (°C)
January	18.137	−21.020	−31.537
February	18.134	−21.102	−31.503
March	18.020	−21.025	−30.363
April	18.029	−21.223	−31.453
May	17.985	−21.280	−32.015
June	17.943	−21.291	−32.596
July	17.947	−21.210	−32.630
August	17.950	−21.132	−32.662
September	18.108	−21.155	−33.238
October	18.208	−21.142	−33.244
November	18.253	−21.070	−32.688
December	18.296	−21.027	−32.120

While this analysis shows that a moving average component is unnecessary, residuals originating from using other DBT data may require a moving average component. The order of the ARMA model is specific to the FSR, which are specific to the original DBT. The residuals of the AR model (DBT^t_{ARR}), shown in Fig. 8, seem randomly distributed around zero with constant variance and no apparent structure or trend throughout the year. This result indicates that both the developed FS and AR models are able to accurately capture the trends and patterns of the original DBT. Both the FS and the residuals will be modified to integrate the desired climate change features into the original DBT as shown in Section 2.1.3.

2.1.3. Implementation of temperature climate change features

Feature One — Increase of average maximum and minimum temperatures. Based on the Representative Concentration Pathway Emissions Scenario 4.5 for the year 2045 for the City of Adelaide, Australia, physical models of climate change predict that the average maximum and minimum DBT for each month will increase as summarised in Table 3. Feature One consists of integrating these values into the meteorological weather data. For instance in January, the average maximum and minimum temperatures are predicted to increase by 1.3 °C and 1.2 °C respectively. If the predicted increase of maximum temperature were equal to that of the minimum temperature, an increase of the monthly average by a value equal to the predicted temperature increase would be sufficient. However, as the predicted increase of maximum temperature differs from that of the minimum temperature within and across different months, an increase of only the monthly average is insufficient to match the predicted values of maximum and minimum temperatures. Therefore the FS is separately modified for each month to achieve the predicted increase.

The modification consists of optimising the monthly mean DBT and the coefficients of the FS model corresponding to daily cycles. As the modification is related to *daily* averages of maximum and minimum temperatures, the coefficients corresponding to seasonal and half–daily cycles are maintained constant in order to reduce unnecessary modifications of the FS. The optimisation minimises the difference between the FS and the modified FS (MFS) for each month separately while achieving the required increase of monthly averages of maximum and minimum temperatures. The optimisation also considers maintaining the time of occurrence of daily maximum temperature in the MFS equal to that of the FS. The optimisation is conducted in Microsoft Excel using the generalized reduced gradient algorithm. The optimised values are summarised in Table 4.

The implementation of Feature One shows that the DBT (MFS) is higher than the DBT (FS); nevertheless, the difference between the two series is not constant as shown in Fig. 9 (i.e. the same week shown in Fig. 3). The difference is relatively large at times corresponding to maximum and minimum temperatures and small at other times. The variable difference clearly indicates that the optimisation includes not only translation but also deformation of the FS while maintaining the same time of occurrences of the daily maximum and minimum temperatures. The difference between the DBT (MFS) and the DBT (FS) is translated to the modified DBT which consists of the residuals of the DBT (FS) plus the DBT (MFS), as shown in Fig. 9.

Feature Two — Adjustment of the number of extreme days. The projected number of days with maximum DBT exceeding 35 °C and 40 °C is 32 and 9 respectively [22]. However, based on the implementation of Feature One, the daily maximum temperature exceeds 35 °C and 40 °C for 28 days and 4 days respectively, as shown in Fig 10. The integration of Feature Two increases the num-

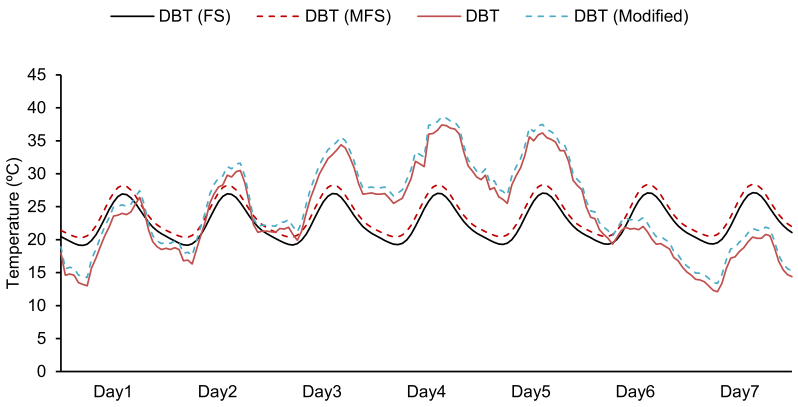

Fig. 9. Dry bulb temperature with modified averages of maximum and minimum daily temperatures (hourly profile for one week).

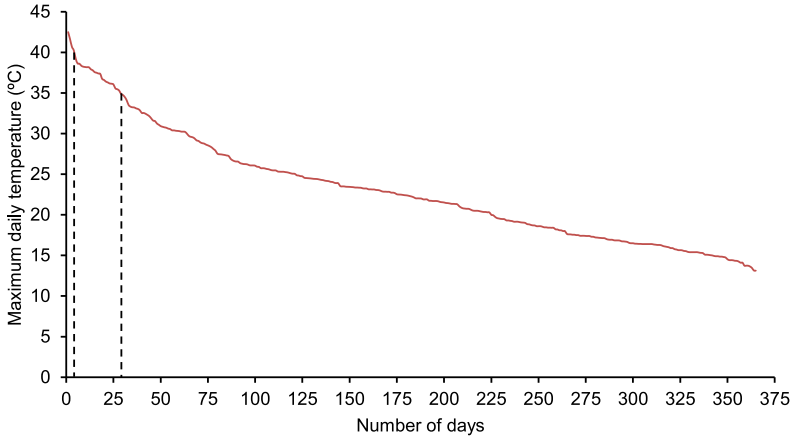

Fig. 10. Cumulative distribution of maximum daily dry bulb temperature.

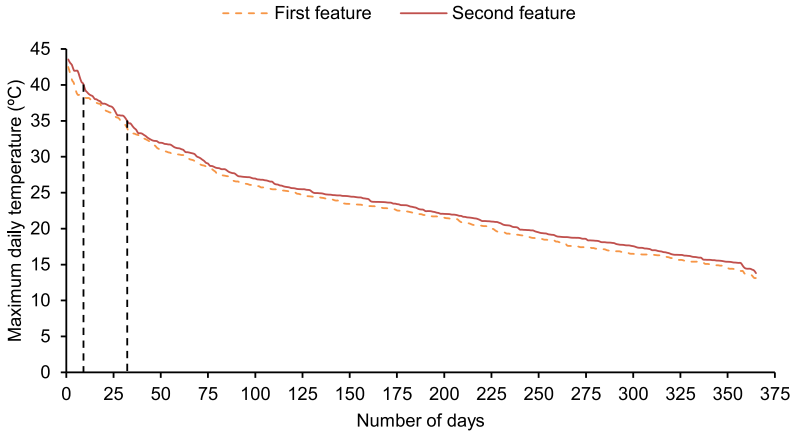

Fig. 11. Comparison of cumulative distributions of maximum daily dry bulb temperature.

ber of days that have the daily maximum temperature above these temperature limits.

The integration of this feature consists of creating a random set of 8760 elements using the residuals of the AR model shown in Fig. 8. The random set is then added to the AR and MFS fits, creating a new hourly DBT set for the entire year. The random selection is repeated until the number of days with maximum daily temperature exceeding 35 °C and 40 °C is 32 and 9 respectively.

The effect of integrating Feature Two is clearly shown in the comparison of cumulative distributions presented in Fig 11. The cumulative distribution with Feature Two is higher than that with Feature One, and the number of days with maximum daily temperature above 35 °C and 40 °C matches the required values, i.e. 32 and 9 respectively.

To identify one year that satisfies Feature Two, a large number of random sets has been generated (10,000 sets). This result reveals the significant difference between the current and future weather patterns. The large number of random sets required indicates that the random selection process may never produce a set that satisfies Feature Two for other DBT data. This condition can occur when the residuals of the ARMA model are small and either the specified temperature thresholds or the number of days with maximum daily temperature exceeding specified temperature thresholds is large. This condition can be overcome by upscaling

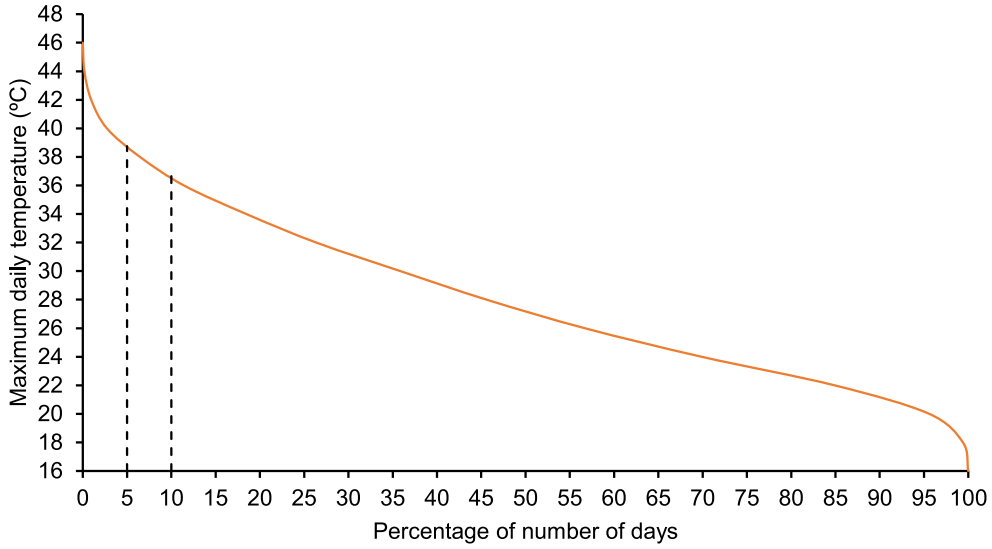

Fig. 12. Distribution of historical daily maximum temperature based on data from [24].

the residuals of the ARMA model to generate sufficiently large residuals for the random selection process. Nevertheless, excessive upscaling is discouraged and researchers should use discretion to maintain a balance between the upscaling factor and the number of randomly selected sets of residuals necessary to identify a suitable year of DBT data.

Feature Three — Integration of heatwave characteristics. Feature Three imposes additional constraints on the days with maximum DBT above specified thresholds. Instead of being sparsely distributed, these days should be successive for a specified period, which can realistically represent a heatwave. According to the Bureau of Meteorology, a heatwave is defined as *three or more days of unusually high maximum and minimum temperatures* [23]. However, this definition is ambiguous as the term *unusually* conveys neither a clear meaning nor precise values of the maximum and minimum temperatures. Therefore, researchers should use discretion to decide the temperature limits considered as *unusually* high. In this research, two heatwave temperature limits are considered, 36.6 °C and 38.7 °C, which correspond to the 90th and 95th percentiles for the daily maximum temperature respectively. Using freely accessible data for the City of Adelaide (Kent Town) from the Bureau of Meteorology [24], the percentiles are calculated considering the warmest months of the year (Dec–Mar) for the period 01/02/1977–16/01/2018. The percentiles and the corresponding maximum daily temperature are shown in the cumulative distribution in Fig. 12.

Consequently, for the integration of Feature Three, at least three consecutive days with maximum DBT above 36.6 °C or 38.7 °C are assumed to represent a heatwave. Based on the integration of Feature Two, the result in Fig. 13 shows two heatwaves with maximum DBT above 36.6 °C. Therefore, for this temperature threshold, the implementation of Feature Two is sufficient to produce heatwaves, and no further modifications are necessary. However, Fig. 13 shows no heatwaves when the heatwave temperature threshold is set to 38.7 °C.

To be able to implement Feature Three, random sampling from the AR residuals follows a Markov chain model (MCM). The aim of this model is to increase the chance of sampling a high AR residual when the last sampled residual is high. This sampling process increases the chance of maintaining higher temperatures, which can eventually produce three consecutive days with daily maximum DBTs over 38.7 °C. However, increasing the chance of sampling high AR residuals shifts the mean of the sampled residuals above zero; creating an undesirable increase of the mean DBT temperature. Therefore, the MCM should also increase the chance of sampling a low AR residual when the last sampled residual is low. The sampling of low AR residuals helps to maintain the mean of the sampled residuals close to zero.

Table 5
Clusters temperature limits.

	C1	C2	C3
High temperature limit (°C)	9.3877	0.8737	-0.3715
Low temperature limit (°C)	0.8766	-0.3710	-8.9336
Number of residuals	1031	5005	2724

Table 6
Transition matrix.

	C1	C2	C3
C1	175	511	345
C2	496	3074	1435
C3	360	1420	943

The MCM is based on three clusters (C1, C2 and C3) of high, medium and low AR residuals respectively. The clusters are created in Matlab using k–means algorithm which iteratively assigns each residual to one of the clusters based on the Euclidean distance of the residual to the mean of each of the three clusters [25]. The residual is then assigned to the cluster corresponding to the shortest Euclidean distance. The limits of AR residuals and the number of elements in each cluster are presented in Table 5.

The AR residuals and clusters allow a transition matrix (TM) to be created, as shown in Table 6. The TM shows the number of times the AR residuals transition between the clusters. For instance, a residual in C1 is followed by a residual in the same cluster 175 times. Similarly, a residual in C2 is followed by a residual in C1 496 times. The TM values across each row reveal that the transitions to C1 are the lowest compared to transitions to C2 and C3. These values provide a possible explanation for the nonexistence of three consecutive days with maximum DBT above 38.7 °C when Feature Two is implemented.

Subsequently, a modified TM (MTM) is developed as shown in Eq. (3), where the TM is transformed to increase the observations corresponding to C1 and C3 as aforementioned. The modifications to the TM are justified as the future climate is likely to be more

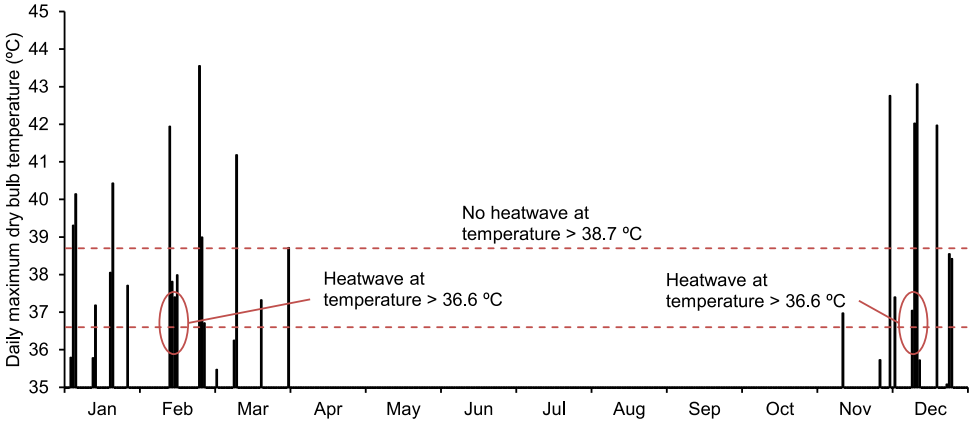

Fig. 13. Distribution of daily maximum temperature throughout the year (using Feature Two).

Table 7
Modified transition matrix.

	C1	C2	C3
C1	425	386	220
C2	621	2824	1560
C3	235	1295	1193

extreme with higher maximum DBTs and longer heatwaves [16]. Other transformations that increase the observations corresponding to C1 and C3 are also possible. Researchers should use discretion to construct a suitable transformation and to select the value of additional observations (AO) to C1 and C3.

$$
\begin{aligned}
MTM(1,1) &= TM(1,1) + AO \\
MTM(1,2) &= TM(1,2) - AO/2 \\
MTM(1,3) &= TM(1,3) - AO/2 \\
MTM(3,3) &= TM(3,3) + AO \\
MTM(3,2) &= TM(3,2) - AO/2 \\
MTM(3,1) &= TM(3,1) - AO/2 \\
MTM(2,2) &= TM(2,2) - AO \\
MTM(2,1) &= TM(2,1) + AO/2 \\
MTM(2,3) &= TM(2,3) + AO/2
\end{aligned} \tag{3}
$$

Based on an AO value of 250, the corresponding MTM is presented in Table 7. This matrix allows a Markov chain of the clusters for the entire year to be generated. The chain value at each hour indicates the cluster used for the sampling of the AR residuals. A one–day sample of the clusters chain and the corresponding AR residuals is presented in Fig. 14. When the clusters chain is C1 for the first five hours, the AR residuals (brown markers) are sampled from C1 which contains the highest residual values. At hour six, a transition from C1 to C2 occurs and the sampling of the AR residual for this hour is from C2.

Using sampled AR residuals based on the generated chain for the entire year, the procedure of integrating Feature Two is applied to identify a set of DBT that satisfies the requirements of both Feature Two and Feature Three. The result in Fig. 15 shows three consecutive days with maximum daily DBT above 38.7 °C in December; creating a heatwave which does not exist in the original DBT data nor in the DBT with Feature One and Feature Two implemented.

Table 8
Predicted change of total solar irradiation.

Month	Change percentage Δ_k (%)
January	0.0
February	0.2
March	−0.1
April	0.4
May	1.1
June	2.5
July	2.4
August	2.3
September	1.7
October	1.5
November	0.7
December	0.4

2.2. Solar irradiation

2.2.1. Implementation of climate change

The change of solar irradiation due to climate change is expressed as percentages of the monthly means of total solar irradiation (I) as shown in Table 8 [21].

Consequently, total solar irradiation that includes climate change (I_{mod}) can be calculated as shown in Eq. (4)

$$I_{mod,k} = I_k \times (1 + \Delta_k/100) \tag{4}$$

where the subscript k refers to the month of the year and Δ_k refers to the corresponding month value in Table 8.

2.2.2. Diffuse and direct normal irradiation

Hourly total solar irradiation for the entire year can be calculated using Eq. (4). Nevertheless, for most applications diffuse irradiation on a horizontal surface (I_d) and direct normal irradiation (I_{dn}) are necessary. For instance, these two solar components are required in TMY weather data used in building energy simulation. The (I_d) and (I_{dn}) values are calculated as shown in Eqs. (5) and (6)

$$I_d = I_{mod} \times f_d \tag{5}$$

$$I_{dn} = (I_{mod} - I_d)/\sin\alpha \tag{6}$$

where f_d and α are the diffuse solar irradiation on horizontal surface and the solar altitude respectively. The calculation details of f_d are presented in [26]. The values of I_{dn} can be unrealistic near sunrise and sunset as α and hence $\sin\alpha$ are close to zero [27]. To eliminate these values, I_d and I_{dn} are adjusted as shown in Eqs. (7) and (8), assuming that solar irradiation is entirely diffuse near

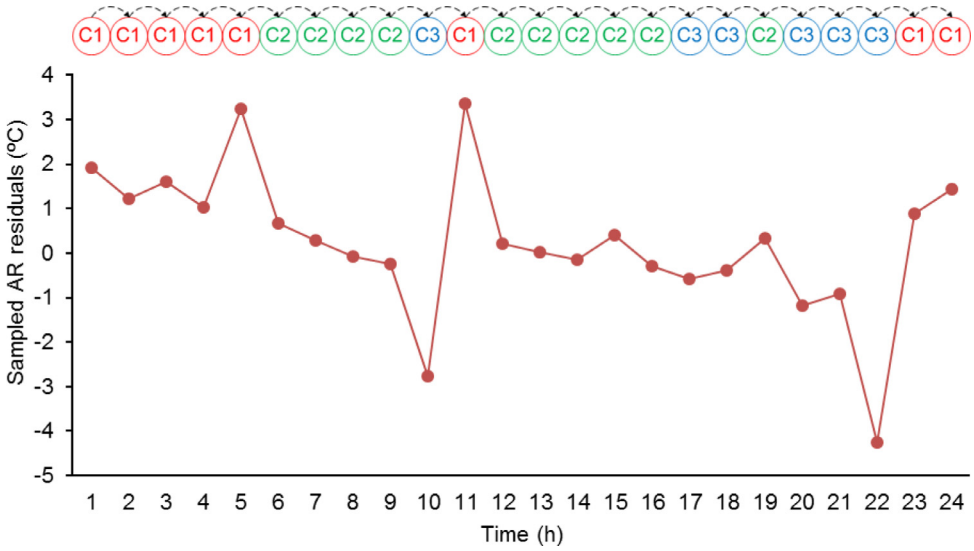

Fig. 14. Clusters chain and corresponding randomly selected residuals.

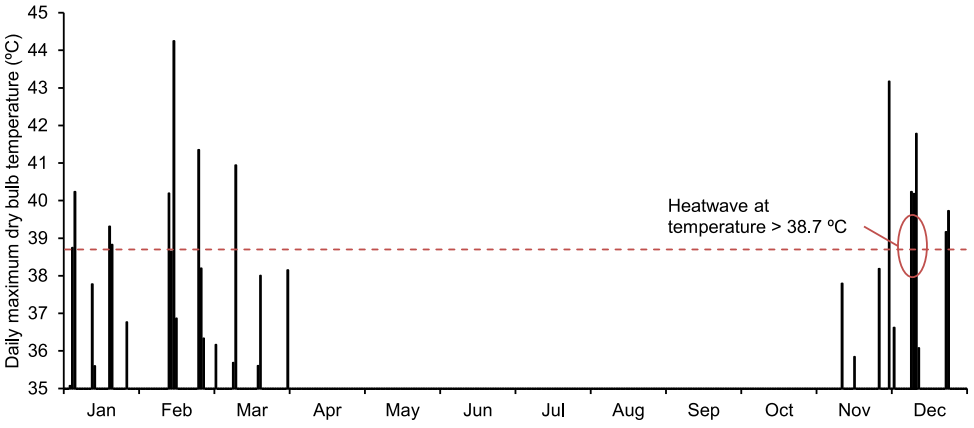

Fig. 15. Distribution of daily maximum temperature throughout the year (using Feature Three).

sunrise and sunset.

$$I_d = I_{mod} \quad \text{if } |\sin\alpha| < 0.05 \tag{7}$$

$$I_{dn} = 0 \quad \text{if } |\sin\alpha| < 0.05 \tag{8}$$

3. Heating and cooling energy performance

The original and developed climate–changed weather data are used in Transient System Simulation software (TRNSYS) to compare heating and cooling energy performances of a single space. The comparison considers total annual thermal energy, maximum hourly thermal power, and maximum daily thermal energy. The total annual thermal energy is associated with the amount and cost of primary energy required, while the maximum hourly thermal power is associated with the required capacity of the heating and cooling system. The maximum daily thermal energy is associated with the capacity of energy storage that can be included in a heating and cooling system. The heating and cooling performances are obtained for set temperatures inside the conditioned space equal to 18 °C and 25 °C for heating and cooling respectively, as these temperatures mimic thermal comfort requirements set by NatHERS for the Adelaide climate zone. Dimensions and envelope thermal properties of the simulated conditioned space can be found in [28].

3.1. Impact on annual thermal energy

The results show that the annual heating thermal energy is practically the same for the climate–changed weather data for all three of the implemented climate change features. More importantly, the climate–changed heating thermal energy is 21%–22% less than that for the original weather data, revealing an expected significant reduction of energy required for space heating, as shown in Fig. 16. Similarly, the climate–changed cooling thermal energy is the same for all three of the implemented climate change features. Also similarly and as expected, the amount of cooling thermal energy increases significantly, 29%–31%, when using climate–changed weather data compared to using the original weather data. Surprisingly, the combined annual thermal energy for heating and cooling, which is what NatHERS assesses, is 4%–5% lower when using the climate–changed weather data compared to using the original weather data. This reduction is associated with the reduction of annual heating thermal energy which is more than double the annual cooling thermal energy. The annual heating thermal energy decreases from 210% of the annual cooling thermal energy for the original weather data to 130% for the climate–changed weather data as shown in Fig. 16. These results indicate that the effect of climate change will reduce the total annual energy demand for space heating and cooling. However, the results do not necessarily indicate that the cost will be reduced for

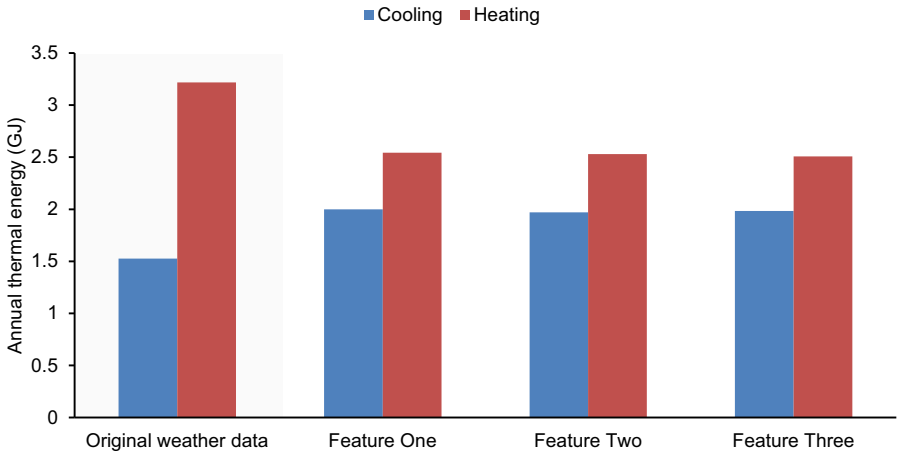

Fig. 16. Comparison of heating and cooling annual thermal energy.

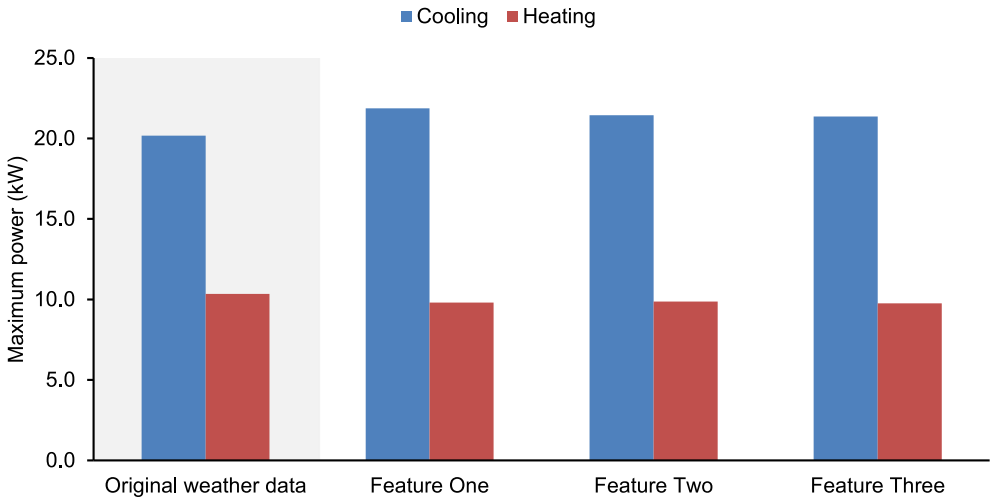

Fig. 17. Comparison of maximum heating and cooling thermal power (hourly resolution).

end–users. For instance, when electricity is used for both heating and cooling, different electricity costs may be applied at different seasons, which may increase the total cost.

3.2. Impact on maximum thermal power

Similar to the annual heating and cooling thermal energy for climate–changed weather data, the maximum heating thermal powers and the maximum cooling thermal powers are practically identical for the different climate–changed weather data as shown in Fig. 17. The climate–changed maximum thermal heating power is slightly lower, 5%–6%, compared to the maximum thermal heating power for the original weather data. In contrast, the climate–changed maximum thermal cooling power is 6%–8% higher than that for the original weather data. Unlike the annual heating and cooling thermal energy, recall Fig. 16 which shows that heating is dominant compared to cooling, the maximum heating and cooling thermal powers show that the cooling power is dominant compared to the heating power. The maximum thermal cooling power for the original weather data is almost double the maximum thermal heating power. This difference further increases as the maximum thermal cooling power increases to 217%–223% of the maximum thermal heating power for the climate–changed weather data.

3.3. Impact on maximum daily thermal energy

The maximum daily heating thermal energy is almost equal for the three integrated features of climate change. The same trend is observed for the maximum daily cooling thermal energy for those features. Nevertheless, the climate–changed maximum daily heating thermal energy is 11%–15% lower compared to the maximum daily heating thermal energy for the original weather data as shown in Fig. 18. A slight increase, 3%–5%, of climate–changed maximum daily cooling thermal energy compared to the maximum daily cooling thermal energy for the original weather data can be observed in Fig. 18. Similar to the hourly heating and cooling maximum thermal powers, the maximum daily heating and cooling thermal energy show that cooling is dominant compared to heating. The maximum daily cooling thermal energy is 63% higher than the maximum daily heating thermal energy for the original weather data. This difference increases to 93%–99% for the climate–changed weather data.

4. Summary and conclusions

Based on data from physical climate change models, this research presented a novel method to integrate multiple features of climate change into meteorological weather data. Using time series analysis, dry bulb temperature (DBT) in the original weather data was separated into multiple components. The time series compo-

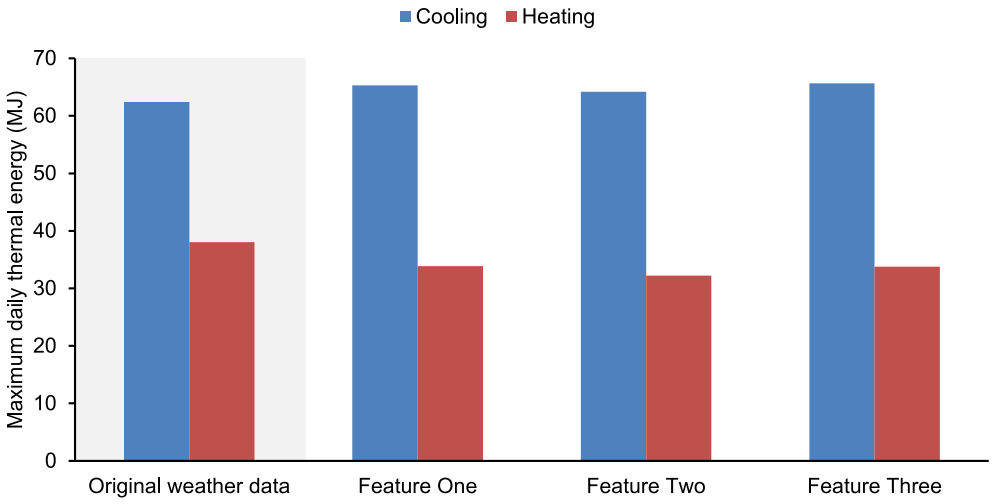

Fig. 18. Comparison of maximum daily heating and cooling thermal energy.

nents were modified to achieve the required DBT features: increase of monthly average of maximum and minimum DBT by different amounts, adjustment of the number of days with the maximum daily DBT higher than a specified threshold, and the number of consecutive days with the maximum daily DBT higher than a specified threshold.

The presented method integrated climate change features that cannot be integrated by the morphing method. However, the presented method is more complex than the morphing method as a thorough analysis of the DBT data is required to develop and modify the time series components. The method also adjusted monthly averages of global solar irradiation, which has an effect on energy usage required for space heating and cooling. Global solar irradiation in the original weather data was shifted by specified monthly values, similar to the morphing method. The modified global solar irradiation was used to calculate diffuse and direct normal irradiation based on an available model for solar diffuse irradiation.

The research also presented the usage of climate–changed weather data by performing an energy analysis based on transient building simulation. The results showed similar energy performances for climate–changed weather data with each of the three different features. Significant differences between energy performances for the original and climate–changed weather data were observed, especially for the annual heating and cooling thermal energy. The annual heating thermal energy decreased by 21%–22% and the annual cooling thermal energy increased by 29%–31%. This result reduced the combined annual heating and cooling thermal energy by 4%–5%.

While the presented integration methods of climate change can be applied to weather data for other locations, the presented energy performance results should not be generalised. The similarity between energy performances for climate–changed weather data could suggest that the integration of Feature Two and Feature Three may be unnecessary for evaluating the annual thermal energy, maximum hourly power and maximum daily thermal energy for space heating and cooling. Nevertheless, the presented results are data and application specific; therefore, analysing the effects of Feature Two and Feature Three should not be prematurely disregarded.

Acknowledgments

This research is supported by an Australian Government Research Training Program (RTP) Scholarship. This research is funded by the CRC for Low Carbon Living Ltd, supported by the Cooperative Research Centres program, an Australian Government initiative. The authors acknowledge the permission of the Commonwealth of Australia to access and use Reference Meteorological Year Climate Files 2016 in this research.

References

[1] Casey Ivanovich, A look back at 2017: the year in weather disasters and the connection to climate change, 2018, (http://blogs.edf.org/climate411/2018/01/03/a-look-back-at-2017-the-year-in-weather-disasters-and-the-connection-to-climate-change/).
[2] The Paris agreement | UNFCCC, (https://unfccc.int/process-and-meetings/the-paris-agreement/the-paris-agreement).
[3] T.R. Karl, K.E. Trenberth, Modern global climate change., Science (New York, N.Y.) 302 (5651) (2003) 1719–1723, doi:10.1126/science.1090228.
[4] D. Sailor, A. Pavlova, Air conditioning market saturation and long-term response of residential cooling energy demand to climate change, Energy 28 (9) (2003) 941–951, doi:10.1016/S0360-5442(03)00033-1.
[5] S. Belcher, J. Hacker, D. Powell, Constructing design weather data for future climates, Build. Serv. Eng. Res. Technol. 26 (1) (2005) 49–61, doi:10.1191/0143624405bt112oa.
[6] A.H. van Paassen, Q.X. Luo, Weather data generator to study climate change on buildings, Build. Serv. Eng. Res. Technol. 23 (4) (2002) 251–258, doi:10.1191/0143624402bt048oa.
[7] J.A. Dirks, W.J. Gorrissen, J.H. Hathaway, D.C. Skorski, M.J. Scott, T.C. Pulsipher, M. Huang, Y. Liu, J.S. Rice, Impacts of climate change on energy consumption and peak demand in buildings: a detailed regional approach, Energy 79 (2015) 20–32, doi:10.1016/J.ENERGY.2014.08.081.
[8] L. Guan, Preparation of future weather data to study the impact of climate change on buildings, Build Environ. 44 (4) (2009) 793–800, doi:10.1016/J.BUILDENV.2008.05.021.
[9] M.J. Scott, L.E. Wrench, D.L. Hadley, Effects of climate change on commercial building energy demand, Energy Sources 16 (3) (1994) 317–332, doi:10.1080/00908319408909081.
[10] BRANZ, An Assessment of the Need to Adapt Buildings for the Unavoidable Consequences of Climate Change, Technical Report, Report to the Australian Greenhouse Office, Department of the Environment and Water Resources, 2007.
[11] J.T. Houghton, Y. Ding, D.J. Griggs, M. Noguer, P.J. van der Linden, X. Dai, K. Maskell, C.A. Johnson, IPCC, 2001: Climate Change 2001: The Scientific Basis. Contribution of Working Group I to the Third Assessment Report of the Intergovernmental Panel on Climate Change, Technical Report, Cambridge University Press, Cambridge, United Kingdom and New York, NY, USA, 2001.
[12] M.J. Holmes, J.N. Hacker, Climate change, thermal comfort and energy: meeting the design challenges of the 21st century, Energy Build. 39 (7) (2007) 802–814, doi:10.1016/j.enbuild.2007.02.009.
[13] M.F. Jentsch, A.S. Bahaj, P.A. James, Climate change future proofing of buildings – generation and assessment of building simulation weather files, Energy Build. 40 (12) (2008) 2148–2168, doi:10.1016/J.ENBUILD.2008.06.005.
[14] X. Wang, D. Chen, Z. Ren, Assessment of climate change impact on residential building heating and cooling energy requirement in australia, Build Environ. 45 (7) (2010) 1663–1682, doi:10.1016/j.buildenv.2010.01.022.
[15] A. Chan, Developing future hourly weather files for studying the impact of climate change on building energy performance in hong kong, Energy Build. 43 (10) (2011) 2860–2868, doi:10.1016/J.ENBUILD.2011.07.003.
[16] W. Steffen L. Hughes, S. Perkins, Heat Waves: Hotter, Longer, More Often, Technical Report, Climate Council of Australian Ltd, 2014.

[17] M. Herrera, S. Natarajan, D.A. Coley, T. Kershaw, A.P. Ramallo-González, M. Eames, D. Fosas, M. Wood, A review of current and future weather data for building simulation, Build. Serv. Eng. Res. Technol. 38 (5) (2017) 602–627, doi:10.1177/0143624417705937.
[18] D.M. Whaley, T. O'Leary, B. Al-Saedi, Cost benefit analysis of simulated thermal energy improvements made to existing older south australian houses, Procedia Eng. 180 (2017) 272–281, doi:10.1016/j.proeng.2017.04.186.
[19] J. Ben Liley, Creation of NatHERS 2016 reference meteorological years, 2017, (http://nathers.gov.au/sites/prod.nathers/files/u20/2016_Climate_File_NIWA_Report.pdf).
[20] W.J. Parton, J.A. Logan, A model for diurnal variation in soil and air temperature, Agricult. Meteorol. 23 (1981) 205–216, doi:10.1016/0002-1571(81)90105-9.
[21] Climate change in Australia, 2017, Accessed: 10/11/2017, (https://www.climatechangeinaustralia.gov.au/en/climate-projections/climate-futures-tool/detailed-projections/).
[22] L. Webb, K. Hennessy, Projections for selected Australian cities, 2015.
[23] Bureau of Meteorology, Australia weather and warnings, (http://www.bom.gov.au/weather-services/about/heatwave-forecast.shtml).
[24] Bureau of Meteorology, Climate Data Online, 2018, (http://www.bom.gov.au/climate/data/).
[25] k-means clustering - MATLAB kmeans - MathWorks Australia, (http://au.mathworks.com/help/stats/kmeans.html).
[26] B. Ridley, J. Boland, P. Lauret, Modelling of diffuse solar fraction with multiple predictors, Renew. Energy 35 (2) (2010) 478–483.
[27] J.A. Duffie, W.A. Beckman, Solar Engineering of Thermal Processes, 4th edition, Wiley, Hoboken, N.J., 2013.
[28] S. Farah, W. Saman, J. Boland, Development of robust meteorological year weather data, Renew. Energy 118 (2018), doi:10.1016/j.renene.2017.11.033.